Magazine of Civil Engineering

ISSN 2712-8172

journal homepage: http://engstroy.spbstu.ru/

DOI: 10.34910/MCE.105.1

The impact of depth on shear behavior of strengthened beams

R. Al-Rousan
Jordan University of Science and Technology, Irbid, Jordan
E-mail: rzalrousan@just.edu.jo

Keywords: reinforced concrete, beam depth, shear, flexural strength, fiber reinforced polymer, nonlinear, finite element analysis

Abstract. The main aim of this work is to investigate the influence of the beam's depth on the behavior of the externally-strengthened-with-CFRP beams, having shear deficiency. The Nonlinear Finite Element Analysis (NLFEA) has been utilized to construct and validate study models, which had been subjected to load till failure aiming to monitor their performance. Also, the cracking's first appearance, the increase rate of cracking according to loadings, and ductility were all put to observation. The NLFEA results indicated that strengthening the RC beams with externally-bonded CFRP enhanced the beams' shear capacity, in accordance to the study parameters. The strips of CFRP enhanced the beam's ultimate load by 15–19 %. In the NLFEA modelled beams, it had been noticed that the more the beam's depth, the less the shear span-to-depth ratio; as that ratio was 2.7 at a depth of 225 mm, where the ratio became 1.2 at a depth of 450 mm. The depth, of strengthened and control beams, was more influential on the beam's ultimate load than the resultant deflections. Also, the attained findings pointed out that the RC beam's depth had affected the cracking angle; as it was: 33°, 44°, 50°, and 54° at a beam's shear span-to-depth ratio of: 2.7, 1.9, 1.5, and 1.2, respectively. Had a shear crack exceeded the length of a CFRP strip, the stirrup would fail to get to its yield strength. In this case, the influence of the beams' depth is limited. Finally, the obtained NLFEA results were evaluated by comparing them to well-known shear strength models.

1. Introduction

For RC beams, the depth of the beam is directly proportional to the shear span. In other words, an increase in the beam's depth results in the shear capacity. It is a common, recommended even, that upon designing RC beams, and the shear capacity must exceed the flexural capacity, to prevent the occurrence of brittle shear failure. Nevertheless, any RC beam could become subjected to lose its shear capacity when it encounters a big variation in the applied loads or steel corrosion, caused by inadequate covering of concrete. Another reason for the RC beam to lose its shear capacity is when it is strengthened in bending. In the light of the lingering issues of RC beams' structural shear capacity and resistance, there must be further researching to come up with proper solutions.

Concrete structures (for example: buildings, bridge decks, girders, offshore structures, parking lots) are subjected to be harmed or damaged because of: improper maintenance, steel corrosion, ageing, faulty design or construction, additional excessive loading such as heavy traffic, the seismic movements, and harsh environmental condition. Due to the old codes of design, or not abiding by the new ones as in some countries, many structures are endangered, and need to be strengthened and/or rehabilitation [1]. It has been reported that 23 % of the concrete bridges in the USA are deficient or not in service [2].

Deficient structure can be repaired or demolished. However, the latter could cause damages, sometimes severe, to the adjacent structures, causing financial losses. Therefore, the need arises to find adequate techniques and materials to strengthen and/or repair such structures. The strengthening

Al-Rousan, R. The impact of depth on shear behavior of strengthened beams. Magazine of Civil Engineering. 2021. 105(5). Article No. 10501. DOI: 10.34910/MCE.105.1

technique of bonding, externally, carbon-fiber reinforced polymer (CFRP) laminates has been widely adopted to repair, strengthen, and rehabilitate deficient or damaged structure [3–6]. The externally-bonded CFRP technique extends the structural life span and serviceability, and decreases the cost and time of maintenance. A great number of researches have highlighted the efficiency of the CFRP material in enhancing the structural flexural strength. When enduring excessive loads, an adequately-designed RC beam possesses a flexural strength enough to guarantee having a flexural failure mode, which is brittle and ductile. Therefore, RC beams must be availed with a satisfactory margin of safety to withstand more critical, sudden modes of failure, such as shear failure. RC beams must be strengthened to improve their shear capacity; and this capacity must be examined upon strengthening a beam in flexure. It is worth mentioning that RC beams shear failures could be disastrous. When overloading a deficient-in-shear-strength RC beam, an abrupt shear failure is likely to take place, with no pre-warning; unlike the flexural failure, which is not sudden in nature, and is proceeded by big cracks and deflections, as pre-warnings. Further, the shear failure mode lessens the structural strength, to a limit less than the flexural capacity, resulting in a significant decrease in ductility. Therefore, it is imperative to enhance the shear capacity of RC beams by proper means of shear strengthening to make sure that the beam's failure mode is the ductile flexural. Among the various types of the fiber-reinforced polymers (FRP) materials, the CFRP one is the most advantageous for its high tensile strength and remarkable fatigue characteristics. FRP materials are widely utilized to rehabilitate and strengthen actually-standing RC structures. That is because these materials have great features, as they are: durable, flexible, ductile, resistant to corrosion, easy to shape and erect, high strength-to-weight ratio, and remarkably resistant to fatigue; making this material highly desired in many RC applications, for example: beams, slabs and columns [3–5]. These properties have made it possible to prolong the life span and the serviceability of structures [1]. The RC structures, commonly, fail or be defected in shear or flexure. Between these two, the deficiency in shear is way more serious because it occurs in sudden, without giving the element the chance to deal with the developed internal stresses. The shear failure could be due to improper designing, reduction in shear reinforcement (RFT) that is caused by steel corrosion or overloading. It has been evident that the use of externally-bonded FRP material's efficiency, in enhances the shear capacity [7–11], is governed, mainly, by its: tensile strength, the ratio of shear reinforcement, the used configuration. In addition, the FRP's efficiency is also affected by: the inclination angle of shear cracks, the concrete's compressive strength, and the yield strength of both the shear reinforcement and steel bars, adding to its ratio of tensile reinforcement. Reinforcing RC structural elements with externally-bonded FRP has been the focus of many researches [12–14]; as several analytical investigations have been carried out to study the strengthened RC beams' shear performance [15–20]. According to these studies, the ultimate shear capacity, of strengthened RC beams, is controlled by; the strength of concrete, the adequacy of steel, and the material's type of the FRP materials.

Although the abundant studies related to the shear behavior of RC beams, there is so little information about the depth of beams, upon the beams' overloading and failure; as this information elaborates the factual condition of the developed stress, the changes of actions, and the mechanisms upon loading. Such information is, urgently, required to better understand the resistance of the concrete and laminates to shear. Further, the detailed formation and distribution of developed strains, throughout the length of the transverse and longitudinal reinforcement, can be employed to adjust the finite element modelling, particularly the bonding adequacy. Keeping in mind the fact that the structural shear strength is formed by the total internal actions together. It is imperative for the numerical model to avail the actual value of each internal action by itself. Hence, this research introduces a new approach that consists of erecting, externally, the CFRP sheets on RC beams that were different in depth. The main aim, of this study, is to examine the influence of shear span-to-depth (a/d) ratio of externally-strengthened-with-CFRP RC beams on the structural shear strength. To achieve this aim, the nonlinear finite element analysis (NLFEA) method has been utilized. The study investigated the impacts of 4 main methods of strengthening, namely: 1) RC beams with a depth of 225 mm (shear span-to-depth ratio of 2.7) strengthened externally with CFRP composite at a spacing of 100 mm, center to center; 2) RC beams with a depth of 300 mm (shear span-to-depth ratio of 1.9) strengthened externally with CFRP composite at a spacing of 100 mm, center to center; 3) RC beams with a depth of 375 mm (shear span-to-depth ratio of 1.5) strengthened externally with CFRP composite at a spacing of 100 mm, center to center; and 4) RC beams with a depth of 450 mm (shear span-to-depth ratio of 1.2) strengthened externally with CFRP composite at a spacing of 100 mm, center to center. Eight models have been built and experimented under four points loading. According to the experimental findings of Shbeeb et al. [21], the models of this research were validated after they had been simulated, utilizing the ANSYS software. The parameter of this study was the depth of the RC beam models.

2. Methods

The NLFEA method is adopted to analyze complicated designs of structures, effectively; as this method is operated on virtual structures, which allows the user to study the effect of any parameter, leading to considerable savings in efforts, time, and cost. Also, this method enables the user to alter any setting or

variable to explore its effect on the structure. Also, it facilitates the ability to record the resultant values, due to the change of load levels, of stresses, strains, and displacements, at any point. To examine the influence of various parameters, six full-scale, strengthened-with-CFRP models were modelled.

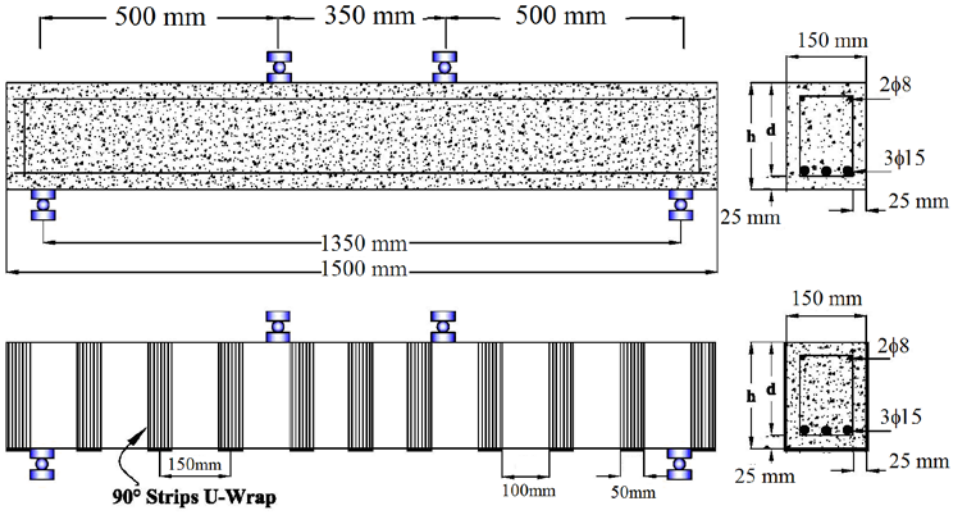

Figure 1. Setup and reinforcement details of the beams [21].

2.1. Experimental Work Review

The finite element models were validated in accordance with the study carried out by Shbeeb et al. [21]. Highly-strengthened RC beams were constructed, dimensioned as 100×150×1400 mm, without being reinforced in shear. Stirrups were put in the zone of constant moment, for the ease of placing the flexural reinforcement, availing a proper concrete confinement, as illustrated in Fig. 1. The experimental specimens consisted of 22 rectangular RC beams, with dimensions of 150×225 mm and a total length of 1500 mm. The top side of the specimens was reinforced with 2ϕ8 bars, 3ϕ15 bars at the lower side, and with stirrups of ϕ8 located at 250 mm, center to center, throughout the beams' total length. The design variables were set to make sure that shear failure would take place within the beams. Four of the specimens were left un-strengthened to be the control, or reference, beams; while the remaining 22 specimens were strengthened with CFRP strips and sheets, in various schemes (Fig. 1). A specially-designed, built-up rigid steel frame was employed to test the specimens, as simply supported. Also, a hydraulic jack was utilized to add an extensive load, within a hydraulic cylinder, to a spread steel beam, so as to generate a two-point loading state, to create an area of constant moment, at mid-span.

2.2. Description of Non-linear Finite Element Analysis (NLFEA)

Concrete seems to be a brittle material, and does not exhibit the same behavior, in compression and tension. SOLID65 was used because it can predict, utilizing the smeared crack approach, the concrete's: nonlinear behavior, failure mode, in addition to the failure in crushing as well as in cracking. To determine the concrete surface failure mode, both the ultimate uniaxial tensile and compressive strengths need to be specified. Hence, it was possible to compute for the default value of the multi-axial stress states that cause concrete failure. For all the specimens: the Poisson's ratio was made 0.2, as most of the previous studies used a value between 0.05 and 0.25; the shear transfer coefficient (β_t) was in the range from 0.0 (no shear transfer) to 1.0 (complete shear transfer). The concrete, used in this work, had a compressive strength of 55 MPa, and an initial young's modulus (E_c) of 35063 MPa.

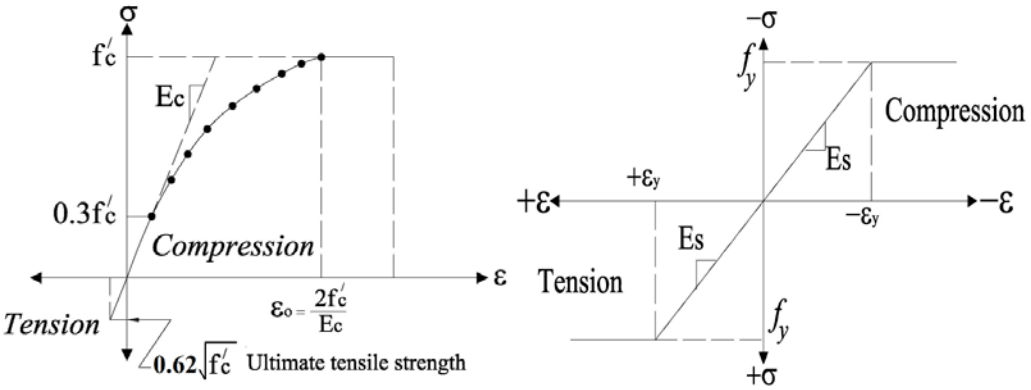

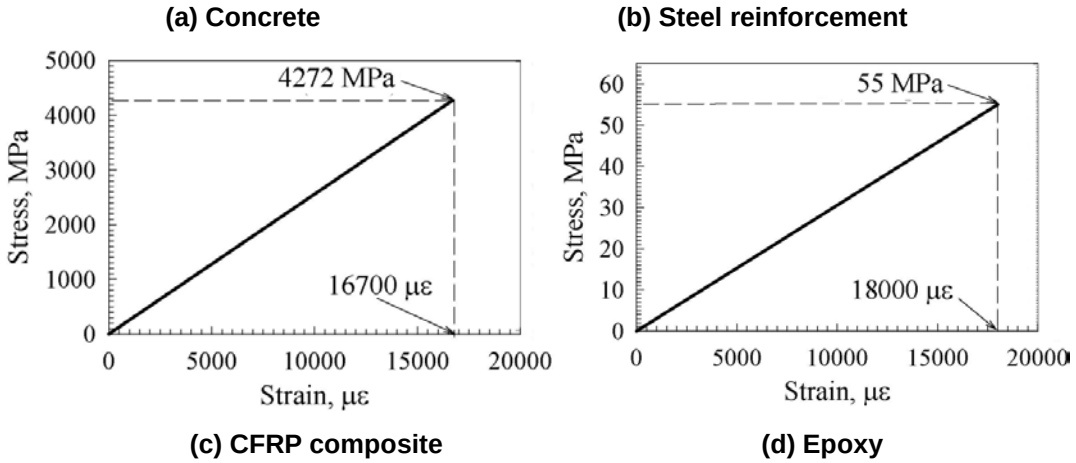

Figure 2. Stress-strain curves [21].

Prior to the point of the ultimate tensile strength, the concrete's stress-strain curve was presumed linear and elastic. Then, cracks emerged in concrete and the strength dropped down, drastically, reaching to zero (Fig. 2). The designed finite element models were reinforced with, presumably an elastic-perfectly plastic, steel, having the same behavior in tension as well as compression. The steel's Poisson's ratio was 0.3, and its yield stress was 413 MPa. Good results were attained upon utilizing the 3D LINK180 uniaxial tension-compression spar in the simulation of the steel reinforcement, separately, to make it possible to predict: the impact of plasticity, huge and rotational stains, and deflections. Fig. 5-2b depicts the relation between the stress and the strain. The two beam's ends were reinforced with steel plates to avail a better distribution of stresses over the support regions. These plates were presumed linearly-elastic, with a modulus of elasticity of 200 GPa, and the Poisson's ratio of 0.3. The SOLID46 element had been used in preparing the adhering material (epoxy) and the, presumably orthotropic, CFRP laminates. The CFRP material had: a thickness of 0.165 mm, a tensile strength of 3790 MPa, an elastic modulus of 228 GPa, and an ultimate tensile strain of 0.017 mm/mm. As the epoxy, it had a thickness of 0.343 mm, the ultimate tensile strength was 55 MPa, the modulus of elasticity of 30 GPa, and the ultimate tensile strain of 0.018 mm/mm. When perpendicular to the direction of the fiber, the CFRP's modulus of elasticity was assumingly 10^{-6} of the main direction. Both the epoxy and the sheets of CFRP had assumingly linearly-elastic characteristics.

The total amount of the exerted load was split to a several load increments; each of which was subjected to the Newton–Raphson equilibrium iterations to be availed with a convergence at its ends, with a tolerance of 0.001. The maximum and minimum sizes of each Load increment were specified, automatically, by ANSYS. As it is stipulated, the concrete structure endures cracking when the main tensile stress is not located inside the failure surface, regardless the direction. Post cracking, the concrete's modulus of elasticity becomes zero, parallel to the prime tensile stress. Concrete crushing takes place, out of the failure surface, when all of the main stresses are compressive. Consequently, the element vanishes and the elastic modulus is set to zero, in all directions. When the concrete's capability of crushing is on, the finite element model fails, in an impulsive manner. Once the concrete's crushing began, it extended in of the areas exposed to direct loads. Then, the neighboring concrete structural elements crushed, as well, leading to a significant decrease in the local stiffness. Lastly, the model exhibited a huge displacement, where the solution diverged. In consequence, the crushing capability was off, and concrete cracking controlled the models' failure. While the concrete was cracking and the emergence of so many cracks, the loads were added, step by step, with smaller increments of load. The models' failure occurred when the load increment of 0.0045 kN did not converge.

CONTA174 element was used to prepare the concrete-epoxy bonding layer. This element is an 8-node element used for analysis in the cases of the general rigid-flexible and flexible-flexible contact. In the general analysis of a contact between two materials or more, the area of contact area cannot be specified in advance. Also, the CONTA174 element is viable for 3-D geometries, and the contact area between solid shells or bodies. Lu et al. [22] introduced the most reliable model of bond stress slip, valid to be included into the finite element analysis. The mechanical behavior of the FRP-concrete bond is described by the relationship between the local shear stress (τ) and the relative displacement (s). In addition, the authors suggested three simplified bond slips, sorted as per their sophistication level, namely: the precise, the simplified, and the bilinear. In the current study, the simplified model (Fig. 3) was adopted for its simplicity.

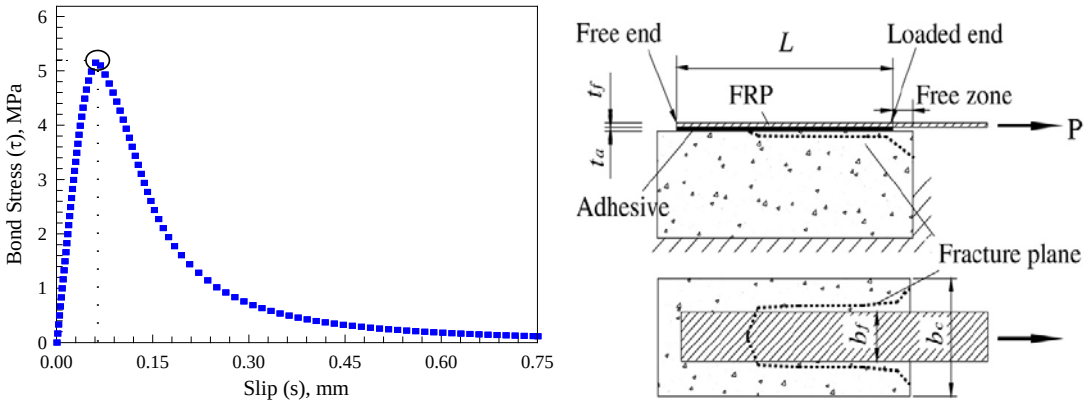

Figure 3. CFRP to concrete bond slip model [22].

The volume-mapped command was utilized to construct rectangular and square structural elements, for the rectangular volumes (concrete, CFRP, epoxy, and steel plates). This facilitates the setting of the steel's length and width to suit the concrete nodes and elements. The suitable mesh density was specified by a convergence study (Fig. 4). Each element was modelled; whereas, the essential concrete meshing measurements were set before the creation of every reinforcement section. The SOLID46 elements, for CFRP and epoxy, had a mesh the same as SOLID65 ones, to ensure that the concrete nodes were allocated over the nodes of each element.

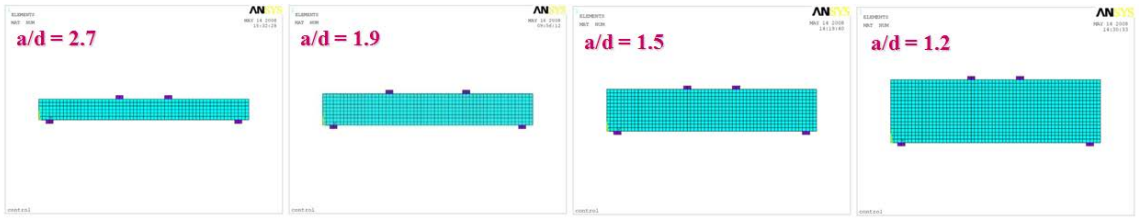

(a) Control beams

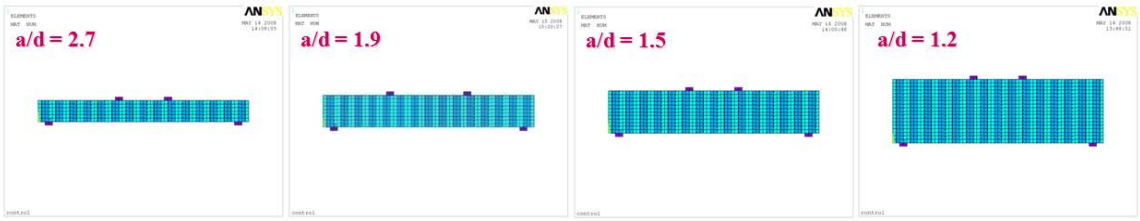

(b) Strengthned beams

Figure 4. Typical finite element meshing of the beams.

The command merge item has been utilized to merge separate entities that are located in the same place, into a single entity. To make sure that the modeling process was done properly, the displacement boundary conditions had been set before they were used at the planes of symmetry; where these planes could be designated by the nodes that defined a certain plane across the beam's cross-sectional section, at the beam's center. To permit the beam to move around the support, a hinge and a roller were installed at the support. The force was exerted throughout the length of the steel plate's centerline. The analysis of the specimens was carried out by simulating a 4-point loading case, at a distance of 550 mm, between the two loading points. The total load had been split to small increments of load, each of which was 0.45 kN. The modified Newton–Raphson equilibrium iterations were utilized to monitor the convergence at every increment's end, with a tolerance margin of 0.001. In order to investigate the specimens' behavior, the static analysis type was used. The model failure took place when the solution of the load increment of 0.0045 kN failed to converge.

2.3. Validation Process

Fig. 5 depicts the load-deflection curves that represent the behavior of both the experimental and NLFEA. Considering Fig. 5, the curves indicated that, for the strengthened specimens, consisted of straight segment indicating the no cracking stage (or pre-cracking); then, there was a variation in the curve's slope, indicating the emergence of cracks (or after-cracking). Continuing raising the exerted load, the strengthened-with-CFRP beams experienced a shear failure, prior to the ultimate flexural capacity limit, as a result of the de-bonding of the CFRP-concrete bond.

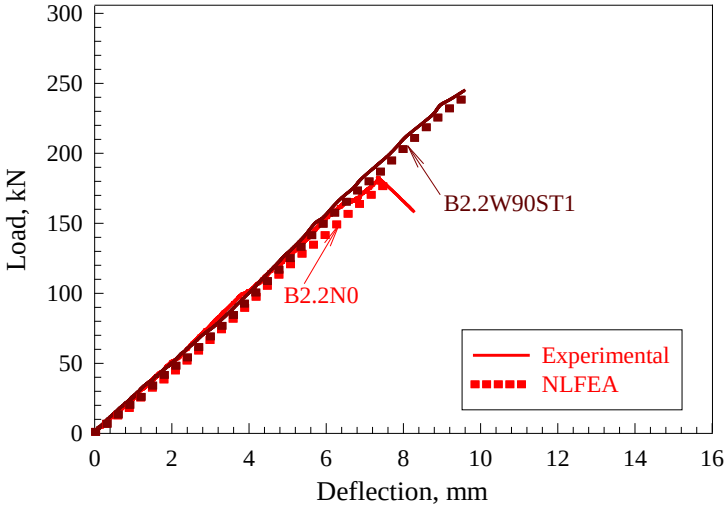

Figure 5. Experimental [21] and NLFEA load-deflection curves.

Referring the obtained values, of the control and strengthened specimens' ultimate strengths and the resultant increase in the ultimate shear strength, indicated that the shear-deficient beams' performance improved due to the CFRP laminates. Considering Fig. 5, the curve of load vs mid-span displacement showed a big agreement between the results of the NLFEA and the experimental ones (with a margin of less than 5 %), when exerting low and high loads. However, at medium loads, there was a slight deviation. This is substantiated by the slight difference between the experimental and the NLFEA's ultimate load, whatever configuration was used. Fig. 6 illustrates typical stress contours of the control and strengthened beams.

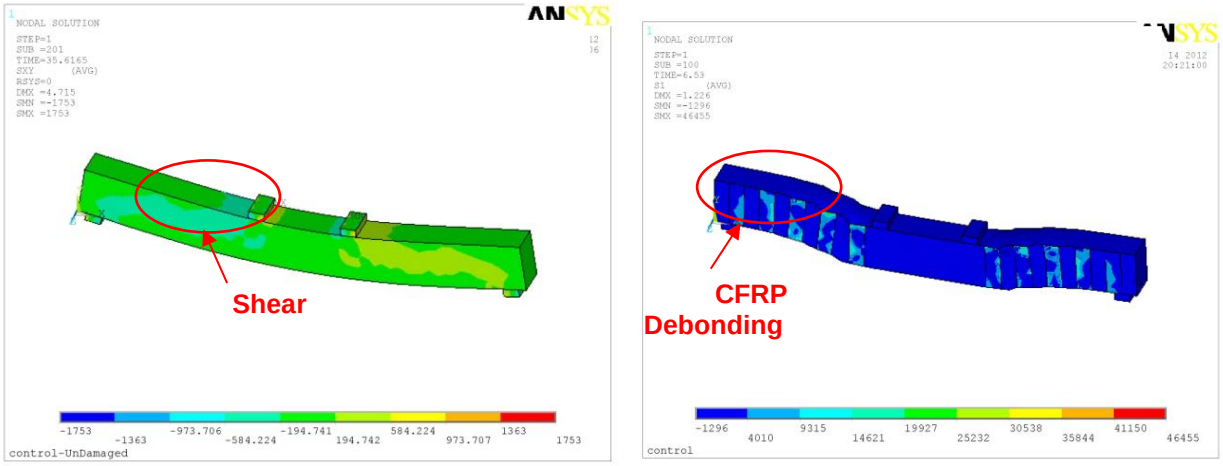

Figure 6. Typical NLFEA stress contours of NLFEA beams.

3. Results and Discussion

3.1. Failure Mode

The control, with no reinforcement, beam specimens had the first flexural crack at the beam's center; later, many cracks appeared away from the mid-section. While raising the exerted load, one of the following cases occurred: either a flexural crack stretched diagonally close to either support, or a diagonal crack emerged suddenly at the beam's mid height, in the shear span region. After the emergence of the diagonal crack, the specimen had a splitting failure, across the tension reinforcement. The mode's type of the ultimate failure was determined by the a/d ratio, and it was either shear or flexural. A representative cracking pattern for the control beams is shown in Fig. 7.

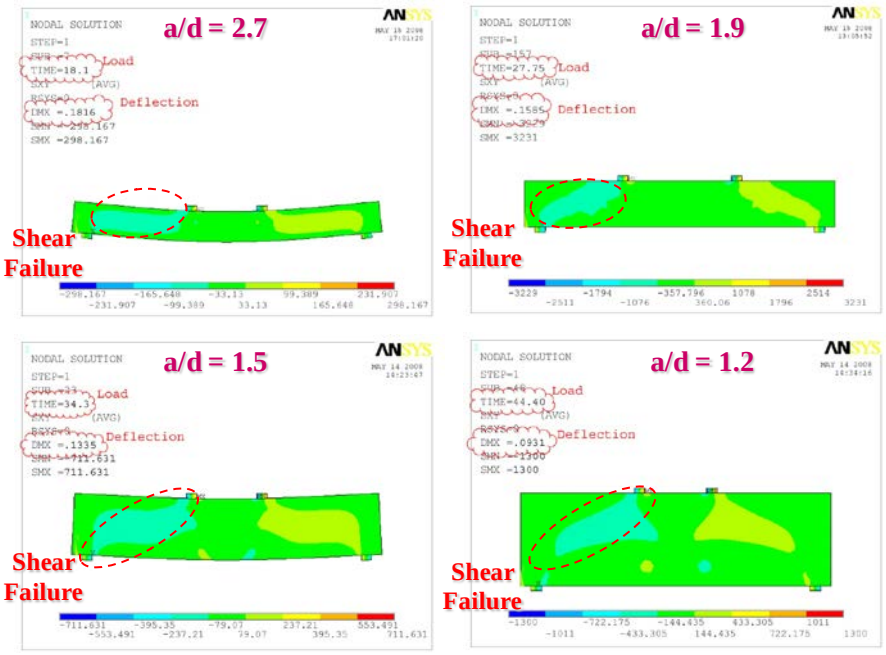

Figure 7. Typical NLFEA stress contours of control NLFEA beams.

Fig. 8 depicts the patterns of cracking of the strengthened NLFEA beam with a/d of 2.7. At a load of 34.2 kN, the first emergence of flexural crack was at the beam's center, inside the constant moment zone. At higher loads, the cracks stretched towards the top fiber; then, more cracks developed, along the length of the beam. At 112.5 kN of load, a shear crack – with an angle of 33°- appeared, not related to the previous ones, at the shear span's center. It was noticed that the strip No. 4 de-bonded at 139.2 kN, followed by strip No. 3 at 142.8 kN. At a load of 146.0 kN, strip No.5 de-bonded, leading to complete failure of the beam, as explicated in Fig. 4 and Table 1. De-bonding is a term that describes the de-lamination of the strip of the CFRP-concrete bond, caused when the bonding strength is higher than the developed stresses, at the end of the strip. Fig. 8 illustrates the patterns of cracking, exhibited by the strengthened NLFEA beam that had an a/d of 1.9. The very first flexural crack emerged at a load of 42.3 kN, at the beam's center, inside the area of constant moment. At a higher load, cracks stretched in the direction of the top fiber. Then, more flexural cracks appeared along the beam. At a load of 124.5 kN, a shear crack, angled at 44°, emerged, not related to the earlier ones, at the shear span's center. The strip No. 4 began to de-bond at 245.0 kN, followed by strip No. 5 at 246.0 kN; then strip No. 2 -closest to the support- de-bonded at a load of 247.2 kN, leading to the beam's shear failure, as illustrated in Fig. 8 and Table 1.

Table 1. The details, ultimate load and mode of failure of NLFEA shear beams.

Beam Designation	h, mm	d, mm	a/d	Type of Strengthening	Ultimate load, kN	Failure mode
B2.7N0	225	185	2.7	None	127.3	Shear failure followed by 33º diagonal crack
B1.9N0	300	263	1.9	None	213.2	Shear failure followed by 44º diagonal crack
B1.5N0	375	333	1.5	None	248.4	Shear failure followed by 50º diagonal crack
B1.2N0	450	417	1.2	None	403.2	Shear failure followed by 54º diagonal crack
B2.7U90ST1	225	185	2.7	Strip@ 90º U-wrap	146.0	Shear failure followed by 33º diagonal crack and debonding of CFRP sheets
B1.9U90ST1	300	263	1.9	Strip@ 90º U-wrap	247.2	Shear failure followed by 44º diagonal crack, debonding of CFRP sheets, and ripping of concrete
B1.5U90ST1	375	333	1.5	Strip@ 90º U-wrap	294.2	Shear failure followed by 50º diagonal crack, debonding of CFRP sheets, and ripping of concrete
B1.2U90ST1	450	417	1.2	Strip@ 90º U-wrap	475.1	Shear failure followed by 54º diagonal crack, debonding of

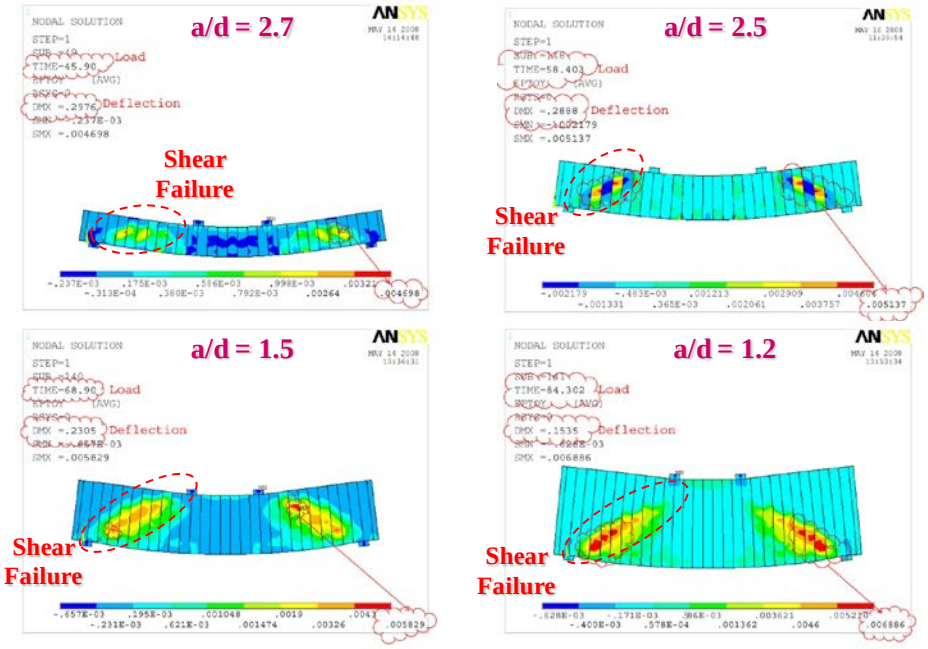

Figure 8. Typical NLFEA stress contours of strengthened NLFEA beams.

Fig. 8 illustrates the cracking patterns, exhibited by the strengthened NLFEA beam, with an a/d ratio of 1.5. The very first emergence of flexural cracks was at a load of 51.6 kN, at the beam's center, in the zone of constant moment. Beyond 51.6 kN, the cracks stretched in the direction of the top fiber. Later, more cracks appeared throughout the length of the beam. At 133.4 kN of load, a shear crack, with an angle of 50°, emerged by itself, in the shear span's center. Upon incrementing the load, the strip No. 4 de-bonded at a load of 287.6 kN, followed by strip No. 5 at 293.4 kN. The beam experienced a shear failure at 294.2 kN, as illustrated in Fig. 8 and Table 1.

Fig. 8 illustrates the cracking patterns exhibited by the strengthened NLFEA beam, with an a/d ratio of 1.2. The first flexural crack appeared at a load of 84.5 kN, at the beam's center, in the zone of constant moment. When exceeding that load, cracks stretched to the top fiber; while, more flexural cracks appeared, along the beam. At a load of 164.6 kN, a shear crack, with an angle of 54°, appeared, separately, at the shear span's center. The strip No. 4 de-bonded at a load of 465.0 kN, followed by strip No. 5 at 475.8 kN. When the load was at 475.1 kN, the beam had a shear failure, as explicated in Fig. 8 and Table 1.

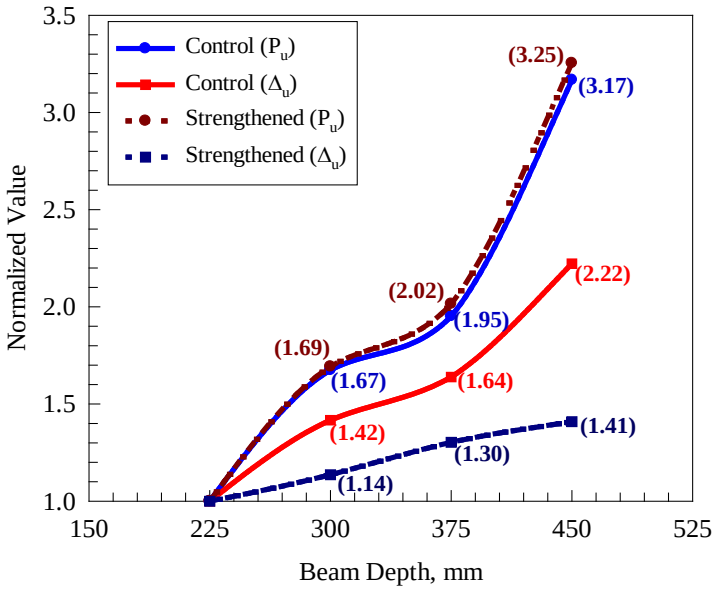

Figure 9. The normalized ultimate load and deflection with respect to control beam.

3.2. Ultimate load capacity

Fig. 9 depicts the strengthened beams' modified ultimate loads and deflections, according to the control beam, having a depth of 225 mm. Referring to Fig. 9, the control beam's ultimate load capacity raised by: 69 %, 102 %, and 225 %, when the depth of the beam increased by: 33 % (300 mm), 67 % (375 mm), and 100 % (450 mm), respectively. The depth's impact on the ultimate load was the same for the strengthened and the control beams. Also, Fig. 9 illustrates that the ultimate deflection, exhibited by the control beams, was higher by: 42 %, 64 %, and 122 %, when the depth was raised by: 33 % (300 mm), 67 % (375 mm), and 100 % (450 mm), respectively. Further, the beam depth's influence on the strengthened beams' ultimate deflection was the same as on the control ones, with enhancement percentages of: 14 %, 30 %, and 41 %, at depths of: 300 mm, 375 mm, and 450 mm, respectively.

3.3. Load-deflection behavior

Fig. 10 illustrates the curves of load vs deflection, for the NLFEA beams. All of the strengthened beams had, nearly, a liner relation between the load and deflection, up to the load of: 129.9, 201.1, 222.8, and 389.2 kN, the same as the failure loads of the beams: B2.7N0, B1.9N0, B1.5N0, and B1.2N0, respectively. This was an indicator that the CFRP conveyed the load after the diagonal shear had developed. Fig. 10 depicts that the beams' ultimate load capacity and beams' stiffness were higher when the effective depth was increased. That was observed by monitoring the angle of rotation, during the elastic phase of the curve, regarding the NLFEA beams. Also, Fig. 10 indicates that the beams' ductility enhanced with the width increase of the anchoring system, which reflected, precisely, the failure mode.

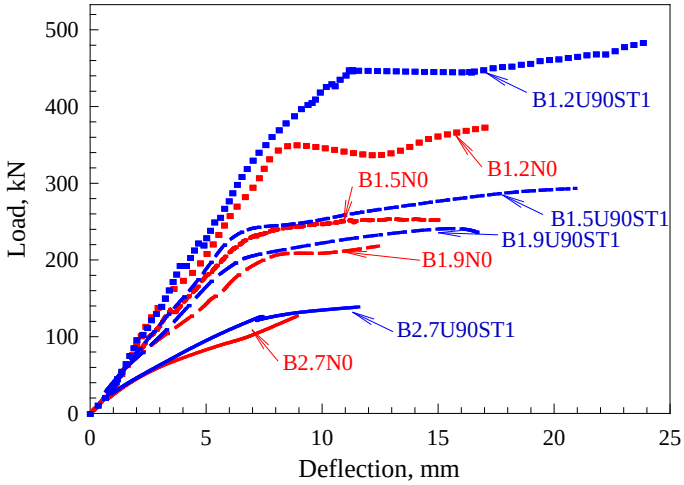

Figure 10. NLFEA load-deflection curves.

3.4. Concrete compressive strain

Fig. 11 depicts the relationship of the NLFEA beam's load and the compressive strain of concrete. Inspecting Fig. 11, it is shown that increasing the beam's effective depth (d) resulted in a rise in the concrete's compressive strength and strain, as well. In general, the highest level of strain was in the strengthened RC beam (B1.2U90ST1).

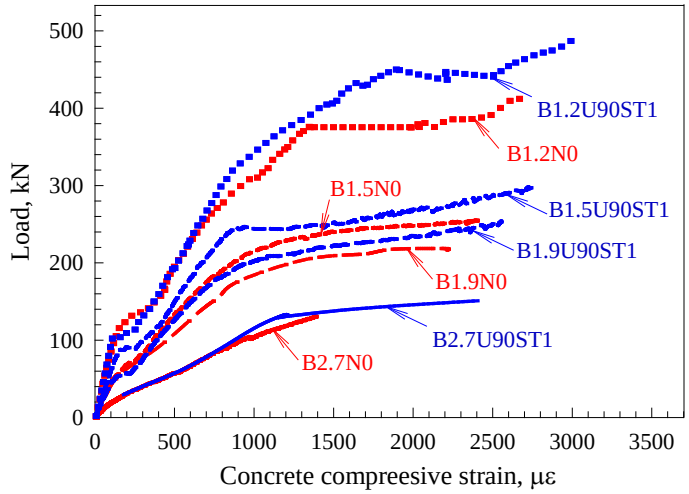

Figure 11. NLFEA load-concrete compressive strain curves.

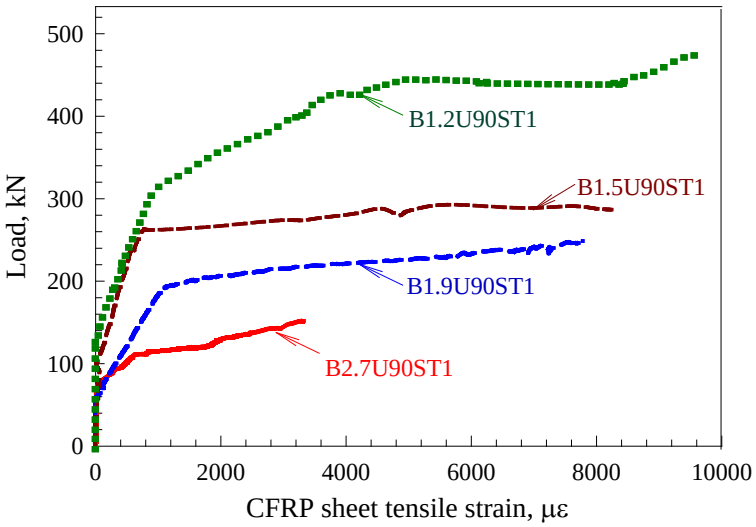

Figure 12. NLFEA load- steel tensile strain curves.

3.5. Steel tensile strain

For NLFEA beams, the curves, that represents the relation between the exerted load and the tensile strain of CFRP sheet, are illustrated in Fig. 12. The curves indicated the emergence of the sheet's tension strain occurred after the formation of the diagonal shear crack, at load levels of: 77.0, 78.3, 79.2, and 84.5 kN, for the beams: B2.7U90ST1, B1.9U90ST1, B1.5U90ST1, and B1.2U90ST1, respectively. In addition, Fig. 12 indicates that the beams: B2.7U90ST1, B1.9U90ST1, and B1.5U90ST1 witnessed sluggish strains, at a load level of 77.8 kN, approximately. Furthermore, Fig. 12 shows that increasing the beam's effective depth (d) resulted in a rise in the tensile sheet strain. In addition, it been found that the reduction of the effective depth delays the emergence of the strain. At the ultimate level of load, the sheets' tensile strains were: 3165$\mu\varepsilon$, 7720$\mu\varepsilon$, 8615$\mu\varepsilon$, and 9640$\mu\varepsilon$, in the beams: B2.7U90ST1, B1.9U90ST1, B1.5U90ST1, and B1.2U90ST1, respectively, equivalent to: 0.19εfu, 0.46εfu, 0.51εfu, and 0.57εfu, respectively. The enhanced values of CFRP strip's strains prove that the using the CFRP bonded length of beam depth is highly efficient in strengthening shear-deficient beams.

3.6. Crack opening behavior

Fig. 13 illustrates the curves of the load vs crack opening, for the NLFEA models. The curves have illustrated that the crack began to widen after the initiation of the diagonal shear cracks, at loads of: 88.5, 109.4, 137.4, 159.2, 98.7, 157.9, 180.6, and 192.2 kN, in the beams: B2.7N0, B1.9N0, B1.5N0, B1.2N0, B2.7U90ST1, B1.9U90ST1, B1.5U90ST1, and B1.2U90ST1, respectively. It was, also, found that, in all beams, the cracks widened to almost 0.25 mm, in a more sluggish manner. The development of cracks was slower in rate when the effective depth (d) was increased. At the ultimate level of load, the ultimate crack width was: 1.78, 2.56, 2.81, 3.07, 1.14, 1.78, 2.43, and 2.71 mm, in the beams: B2.7N0, B1.9N0, B1.5N0, B1.2N0, B2.7U90ST1, B1.9U90ST1, B1.5U90ST1, and B1.2U90ST1, respectively; while the beam B2.7U90ST1 exhibited a less crack width under the same load.

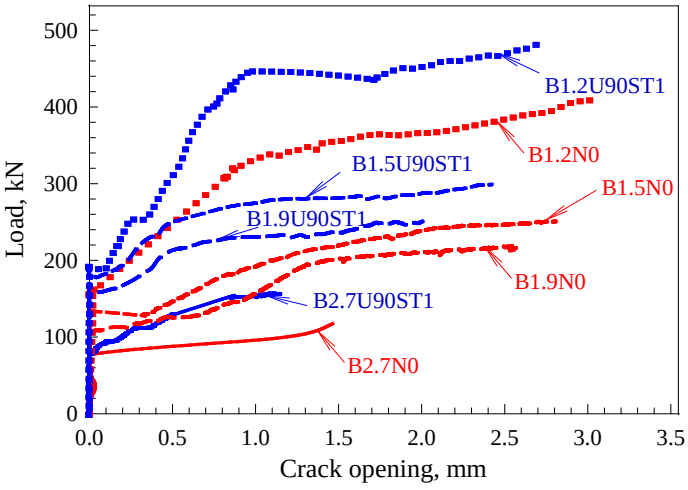

Figure 13. NLFEA load-crack opening curves.

Table 2. Comparison of results obtained with different models.

Beam Designation	NLFEA Ultimate load, kN	Chen and Teng model [23] ($\frac{V_{f,NLFEA}}{V_{f,\mathrm{mod}}}$)	Chen et al. model [24] ($\frac{V_{f,NLFEA}}{V_{f,\mathrm{mod}}}$)	ACI 440.2R model [25] ($\frac{V_{f,NLFEA}}{V_{f,\mathrm{mod}}}$)
B2.7N0	127.3	0.932	0.942	2.058
B1.9N0	213.2	0.923	0.933	2.038
B1.5N0	248.4	0.990	1.000	2.186
B1.2N0	403.2	1.000	1.010	2.208
B2.7U90ST1	146.0	1.011	1.021	2.232
B1.9U90ST1	247.2	0.914	0.924	2.019
B1.5U90ST1	294.2	0.980	0.990	2.163
B1.2U90ST1	475.1	0.941	0.951	2.078
Average	----	0.962	0.971	2.123
CoV (%)	----	37	40	98

3.7. Comparison of NLFEA with theoretical models

For all of the theoretical modeling methods, the first step had to be validated to confirm the methods' efficiency, and to prove their ability of prediction, against the so many experiments, conducted on beams with different properties, geometrically and mechanically, e.g.: the strength of concrete, and the reinforcement quantity and strength, internally and externally. The proposed model has been applied to experimental results as well as the literature test results. The NLFEA model was compared with ACI model, in terms of the obtained results. It was obvious that the guidance of the ACI model had been extracted from the NLFEA data, and they were, only, valid for the external FRP reinforcement. The results of the experimental validation are discussed below.

The comparison, conducted between NLFEA and other analytical methods, namely: Chen and Teng model [23], Chen et al. model [24], and ACI model [25]), as illustrated in Table 2. It is worth noticing that the ACI model was adjusted to the CFRP; whereas, this method must be utilized, cautiously, with other materials. The predictions of the ACI model were not as acceptable, when the mean value ($V_{f,exp}/V_{f,ACI}$) of 2.122, and a COV of 98 %. Referring to Table 2, the models of Chen and Teng [23] and Chen et al. [24] models were better in predicting the NLFEA data. Therefore, Chen and Teng [23] and Chen et al. [24] models have been found to be viable for the externally-bonded beams, regardless the material used (steel or CFRP).

4. Conclusions

1. The CFRP composites technique has proven a great efficiency in improving the RC beams' shear capacity. The externally-bonded CFRP laminates enhance, greatly, the beam's shear capacity to be 15–19 % more than control beams, based on the study parameters.

2. The most monitored mode of failure, of beams strengthened with CFRP strips, was the de-bonding of two or more strips. The test results, of this study, indicated that the de-bonding failure could be avoided by increasing the length of the CFRP strips, at the top side of the beam.

3. The study results pointed out that the depth of the beam depth affected the angle of the main crack; as this angle was: 33, 44, 50, and 54, for the beam's a/d of: 2.7, 1.9, 1.5, and 1.2, respectively.

4. In control and strengthened beams, the beam depth affected the ultimate load more than it did on the deflection.

5. Rising the RC beam's effective depth from 185 mm to 417 mm (corresponding to an a/d ratio of 2.7 to 1.2) reduced the average interface bond stress, and enhanced the effective CFRP sheet's strain, at failure. This had delayed, or even eliminated, the de-bonding failure, and raised the shear capacity, compared with the un-anchored, U-wrapped beams.

6. The extent of the main cracks' inclination affected the shear strength, affecting, in consequence, the overall strength. This study has shown that the shear crack angle had a big role in determining the number of CFRP strips that could be crossed by the crack, and whether the crossed strips were highly effective, or not.

References

1. Ahmed, A., Kodur, V. The experimental behavior of FRP-strengthened RC beams subjected to design fire exposure. Engineering Structures. 2011. 33(1). Pp. 2201–2211. DOI: 10.1016/j.engstruct.2011.03.010
2. Mabsout, M, Tarhini, K, Jabakhanji, R, Awwad, E. Wheel load distribution in simply supported concrete slab bridges. J Bridge Eng. 2004. 9(2). Pp. 293–306. DOI: 10.1061/(ASCE)1084-0702(2004)9:2(147)
3. Al-Rousan, R., Abo-Msamh, I. Bending and torsion behaviour of CFRP strengthened RC beams. Magazine of Civil Engineering. 2019. 92(8). Pp. 48–62. DOI: 10.18720/MCE.92.4
4. Al-Rousan, R. Behavior of two-way slabs subjected to drop-weight. Magazine of Civil Engineering. 2019. 90(6). Pp. 62–71. DOI: 10.18720/MCE.90.6
5. Al-Rousan, R. The impact of cable spacing on the behavior of cable-stayed bridges. Magazine of Civil Engineering. 2019. 91(7). Pp. 49–59. DOI: 10.18720/MCE.91.5
6. Yu, B., Kodur, V.K.R. Fire behavior of concrete T-beams strengthened with nearsurface mounted FRP reinforcement. Engineering Structures. 2014. 80(1). Pp. 350–361. DOI: 10.1016/j.engstruct.2014.09.003
7. Triantafillou, T.C. Antonopoulos CP. Design of concrete flexural members strengthened in shear with FRP. J Compos Constr. 2000. 4(4). Pp.198–205. DOI: 10.1061/(ASCE)1090-0268(2000)4:4(198)
8. Bousselham, A., Chaallal, O. Shear strengthening reinforced concrete beams with fiber-reinforced polymer: assessment of influencing parameters and required research. ACI Struct J. 2004. 101(2). Pp. 219–227. DOI: 10.14359/13019
9. Belarbi, A., Bae, S., Brancaccio, A. Behavior of full-scale RC T-beams strengthened in shear with externally bonded FRP sheets. Constr Build Mater. 2012. 32(1). Pp. 27–40. DOI: 10.1016/j.conbuildmat.2010.11.102
10. Khalifa, A., Nanni, A. Improving shear capacity of existing RC T-section beams using CFRP composites. Cem Concr Compos. 2000. 22(1). Pp. 165–174. DOI: 10.1016/S0958-9465(99)00051-7
11. Mosallam, A., Banerjee, S. Shear enhancement of reinforced concrete beams strengthened with FRP composite laminates. Composites: Part B. 2007. 38(1). Pp. 781–93. DOI: 10.1016/j.compositesb.2006.10.002
12. Ashrafuddin, M., Baluch, M.H., Sharif, A., Al-Sulaimani, G.J., Azad, A.K., Khan, A. Peeling and diagonal tension failures in steel plated R/C beams. Constr Build Mater. 1999. 13(1). Pp. 459–467. DOI: 10.1016/S0950-0618(99)00044-6
13. Rangan, B.V. Shear design of reinforced concrete beams, slabs and walls. Cem Concr Compos. 1998. 20(1). Pp. 455–464. DOI: 10.1016/S0958-9465(98)00027-4
14. Spadea, G., Bencardino, F., Swamy, R.N. Optimizing the performance characteristics of beams strengthened with bonded CFRP laminates. Mater Struct. 2000. 33(1). Pp. 1119–1126. DOI: 10.1007/BF02484166
15. Malek, A.M., Saadatmanesh, H. Ultimate shear capacity of reinforced concrete beams strengthened with web-bonded fiber-reinforced plastic plates. ACI Struct J. 1998. 95(4). Pp. 391–399. DOI: 10.14359/555
16. Triantafillou, T.C. Shear strengthening of reinforced concrete beams using epoxy-bonded FRP composites. ACI Struct J. 1998. 95(2).Pp. 107–115. DOI: 10.14359/531
17. Khalifa, A., Nanni, A. Improving shear capacity of existing RC T-section beams using CFRP composites. J Cem Concr Compos. 2000. 22(2). Pp.165–174. DOI: 10.1016/S0958-9465(99)00051-7
18. Hutchinson, R.L., Rizkalla, S.H. Shear strengthening of AASHTO bridge girders using carbon fiber reinforced polymer sheets. ACI Special Publications (SP-188). 1999. 188(1). Pp. 945–958. DOI: 10.14359/5692
19. Zhang, Z., Hsu, C.T. Shear strengthening of reinforced concrete beams using carbon-fiber-reinforced polymer laminates. J Compos Constr. 2005. 9(2). Pp. 158–169. DOI: 10.1061/(ASCE)1090-0268(2005)9:2(158)
20. Monti, G., Liotta, M.A. Tests and design equations for FRP-strengthening in shear. Constr Build Mater. 2007. 21(24). Pp. 799–809. DOI: 10.1016/j.conbuildmat.2006.06.023
21. Shbeeb, N.I., Al-Rousan, R., Issa, M.A., Al-Salman, H. Impact of bonded carbon fibre composite on the shear strength of reinforced concrete beams. Proceedings of the Institution of Civil Engineers: Structures and Buildings. 2018. 171(5). Pp. 364–379. DOI: 10.1680/jstbu.16.00145
22. Lu, X.Z., J.G. Teng, L.P., Ye, J.J. Jiang. Bond–slip models for FRP sheets/plates bonded to concrete. Engineering Structures Journal 2005. 27 (1). Pp. 920–937. DOI: 10.1016/j.engstruct.2005.01.014
23. Chen, J.F., Teng, J.G. Shear capacity of FRP strengthened RC beams: FRP debonding. Construction and Building Materials. 2003b. 17(1). Pp. 27–41. DOI: 10.1016/S0950-0618(02)00091-0
24. Chen, G.M., Teng, J.G., Chen, J.F. Shear strength model for FRP-strengthened RC beams with adverse FRP-steel interaction. Journal of Composites for Construction, ASCE. 2013. 17(1). Pp. 50–66. DOI: 10.1061/(ASCE)CC.1943-5614.0000313
25. ACI Committee 440. Design and Construction of Externally Bonded FRP Systems for strengthening Concrete Structures. *ACI440.2R-02. 2002. American Concrete Institute, Farmington Hills, Mich.: 45 p. DOI: 10.1061/40753(171)159. ISBN: 9780870312854

Contacts:

Rajai Al-Rousan, rzalrousan@just.edu.jo